ADVANCED FUNCTIONAL MATERIALS
www.afm-journal.de

Low Temperature Stabilization of Nanoscale Epitaxial Spinel Ferrite Thin Films by Atomic Layer Deposition

Mariona Coll, Josep M. Montero Moreno, Jaume Gazquez, Kornelius Nielsch, Xavier Obradors, and Teresa Puig*

In this work heteroepitaxial stabilization with nanoscale control of the magnetic Co_2FeO_4 phase at 250 °C is reported. Ultrasmooth and pure Co_2FeO_4 thin films (5–25 nm) with no phase segregation are obtained on perovskite $SrTiO_3$ single crystal (100) and (110) oriented substrates by atomic layer deposition (ALD). High resolution structural and chemical analyses confirm the formation of the Co-rich spinel metastable phase. The magneto-crystalline anisotropy of the Co_2FeO_4 phase is not modified by stress anisotropy because the films are fully relaxed. Additionally, high coercive fields, 15 kOe, and high saturation of magnetization, 3.3 μ_B per formula unit (at 10 K), are preserved down to 10 nm. Therefore, the properties of the ALD-Co_2FeO_4 films offer many possibilities for future applications in sensors, actuators, microelectronics, and spintronics. In addition, these results are promising for the use of ALD compared to the existing thin-film deposition techniques to stabilize epitaxial multicomponent materials with nanoscale control on a wide variety of substrates for which the processing temperature is a major drawback.

1. Introduction

The ability to stabilize materials of predicted technological and fundamental interest is a major challenge in materials science. Spinel ferrite oxides are one of the most studied compounds among the spinel family owing to their numerous and promising applications in microelectronics, spintronics, sensors, catalysis, and even photoconductivity.[1–5] The cation distribution in these structures can differ depending on the preparation method and it is responsible for the rich variety of physical and chemical properties.[1,6] Among them, cobalt substituted spinel ferrites (with general formula AB_2O_4) are particularly attractive because of the magnetic anisotropy incorporated by the Co ion.[7–9] However, the experimental work on Co-rich ferrite phases is rather scarce due to the difficulty to obtain stable phases by conventional synthetic methods, such as the use of high pressure or soft-chemistry.[2,7,10–14] Another well-known stabilization approach is the synthesis of epitaxial thin films, although a high temperature process is usually required.[15–17] Therefore, a remarkable innovation would be the epitaxial stabilization at low temperature with atomic-level control of metastable spinel ferrite oxide phases, which may have a direct impact on many critical film parameters including roughness, atomic interdiffusion, strain, and structure reconstructions allowing unique structural, magnetic, and electronic properties. In spintronic applications, for instance, keeping high quality interfaces and insulating behavior in ultrathin films without shorts is essential for direct tunneling across the band gap.[18] Tunneling magnetoresistance efficiency is actually dependent on the specific band structure and thus, achieving the novel spinel Co_2FeO_4 with a modified band structure opens new perspectives in this field.[8,18] Furthermore, this would significantly reduce the fabrication cost while making it compatible with a broad range of materials without jeopardizing the system stability.

Atomic layer deposition (ALD) is a unique gas-phase deposition technique that has become a mainstream technology for the production of ultrathin coatings with a high degree of thickness control and a well-defined chemical reaction without non-volatile side products. It is distinguished from other deposition methods for its low temperature and low vacuum deposition conditions, and excellent conformality at the nanometer-scale level.[19–21] A fast-growing development of the ALD process for ternary and quaternary oxides has taken place recently, although it is hampered by the difficulty to find suitable metalorganic precursors for the ALD deposition conditions.[21–27] Spinel phases, such as $ZnAl_2O_4$[28,29] or the Fe-rich cobalt ferrite $CoFe_2O_4$,[11,30–32] have been successfully prepared by ALD as thin films and nanotubes. However, the vast majority of ALD processes at low deposition temperature lead to amorphous or polycrystalline phases.[33] It is noteworthy that it has been recently demonstrated that epitaxial binary oxides can be obtained on chemically compatible single crystal substrates below 300 °C.[34–37] However, thus far, no epitaxial multicomponent oxide thin films have been demonstrated by ALD at reasonably low processing conditions unless a post annealing treatment was performed.[26,38,39]

Dr. M. Coll, Dr. J. Gazquez,
Prof. X. Obradors, Prof. T. Puig
Institut de Ciencia de Materials
de Barcelona (ICMAB-CSIC)
Campus UAB
08193, Bellaterra, Catalonia, Spain
E-mail: mcoll@icmab.es
Dr. J. M. Montero Moreno, Prof. K. Nielsch
Institute of Applied Physics
University of Hamburg
Jungiusstr. 11, 20355, Hamburg, Germany

DOI: 10.1002/adfm.201400517

In this work, we demonstrate the heteroepitaxial stabilization with nanoscale control of magnetic Co_2FeO_4 (CFO) thin films at 250 °C by atomic layer deposition, providing a fascinating opportunity to design and explore novel physical and chemical phenomena. ALD-CFO films with different thicknesses (5–25 nm) have been prepared on perovskite $SrTiO_3$ (STO) single crystal (100) and (110) oriented substrates keeping the same crystalline orientation ($\varepsilon = 7.4\%$). By means of high resolution X-ray diffraction (HR-XRD) and transmission electron microscopy (TEM), the formation of pure, epitaxial and fully relaxed CFO thin films on STO single crystals with no phase segregations has been identified, contrary to what is usually observed when the bulk synthesis is performed.[10,12] Atomic force microscopy studies revealed the formation of ultrasmooth surfaces. The chemical composition and film stoichiometry have been studied by ex-situ X-ray photoelectron spectroscopy (XPS). In-plane and out-of-plane magnetic hysteresis loops for the 25–10 nm CFO thin films, performed at 10 and 300 K, show no modification of the magneto-crystalline anisotropy, which is related to the fact that the films are fully relaxed. High coercive fields and a high magnetization of saturation are identified at 10 K. A strong decrease of the coercivity is observed at 300 K. Also, the 5 nm ultrathin films show a small shrinking of the hysteresis loops at low fields and a weak reduction of the magnetization of saturation, which we attribute to the presence of structural defects, i.e., antiphase boundaries, within the spinel structure.

2. Results and Discussion

Figure 1a,b shows X-ray diffraction (XRD) θ-2θ scans of as-deposited 15 nm CFO films on (a) STO (100) and (b) STO (110). The 2θ values of the Bragg reflections at 44.1° identified in Figure 1a and at 63.5° in Figure 1b suggest the formation of Co_2FeO_4 in both cases. Also, the presence of only (00l) CFO Bragg reflections in (a) and only (011) CFO reflections in (b) confirm the epitaxial growth of ALD-CFO films at 250 °C with no evidence of any secondary phases (see Supporting Information, Figure S2). The out-of-plane orientation of the CFO films is evaluated from the ω-scan, insets in Figure 1a,b. The corresponding rocking curves lead to full width at half maximum (FWHM) values of ≈1.5°, indicating good heteroepitaxy. Remarkably, no such epitaxial quality, phase purity, and stability in Co_2FeO_4 thin film compounds at 250 °C has been previously reported.[11,31]

From high resolution in-plane φ-2θ area scans, the strain and out-of-plane lattice parameter has been analyzed for 15 nm CFO on STO (100), Figure 1c, 5 nm CFO on STO (100), Figure 1d, and 5 nm CFO on STO (110), Figure 1e. The CFO (440) reflection has been studied for the CFO films on (100) STO, whereas the CFO (400) reflection has been studied for the CFO film on (110) STO. The in-plane φ-2θ area scans support the epitaxial relationship previously identified for the two systems, (100)[001]CFO||(100)[001]STO and (110)[011]CFO||(110)[011]STO. By carefully analyzing the c parameter from Figure 1c–e, it has been found to be 8.24(8) Å, 8.26(2) Å, and 8.23(1) Å, respectively. These unit cell dimensions are in good agreement with the reported bulk value of Co_2FeO_4 (c = 8.242 Å) and rules out the formation of the Fe-rich $CoFe_2O_4$ phase (c = 8.381 Å). The minimal divergence (<0.2%) of the c parameter of the obtained ALD- Co_2FeO_4 films from that of the bulk phase suggests the formation of fully relaxed films. The strain state of these ALD-CFO thin films is dramatically different from the $CoFe_2O_4$ oxide spinels prepared at higher temperature by sputtering, pulsed laser deposition, molecular

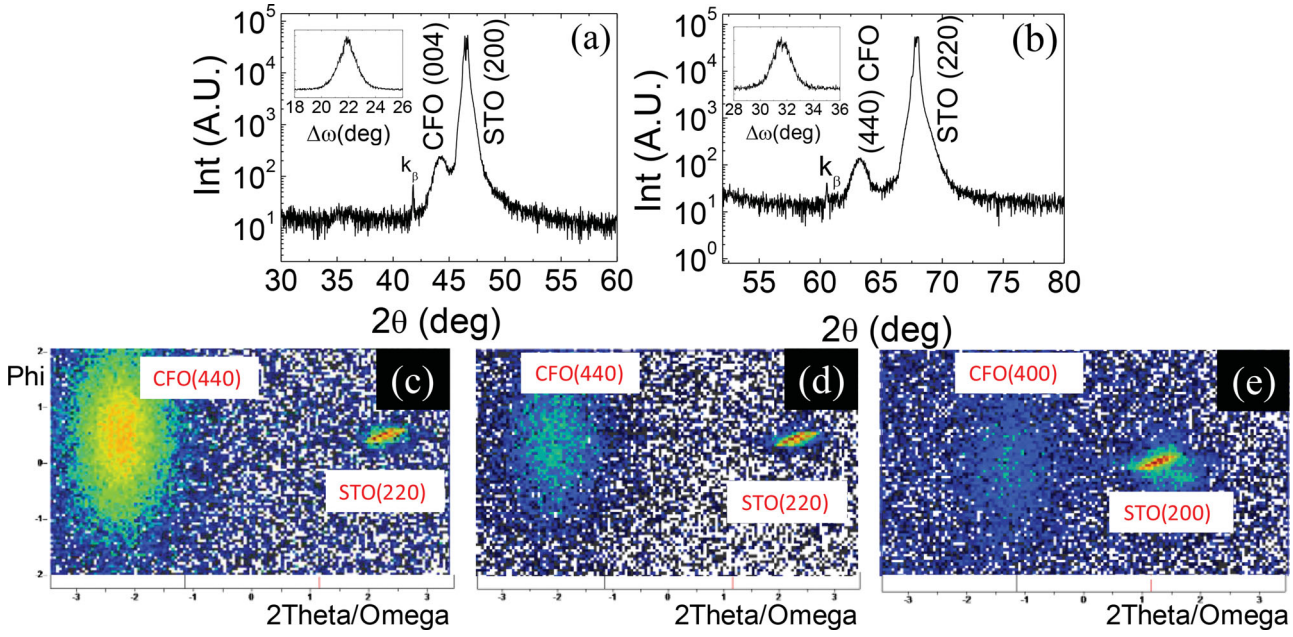

Figure 1. X-ray diffraction θ-2θ scans of as-deposited 15 nm CFO films on a) STO(100) and b) STO(110). High resolution in-plane φ-2θ area scans of c) 15 nm CFO on STO(100) performed around the CFO(440) reflection, d) 5 nm CFO on STO(100) around the CFO(440) reflection, and e) 5 nm CFO on STO(110) around the CFO(400) reflection.

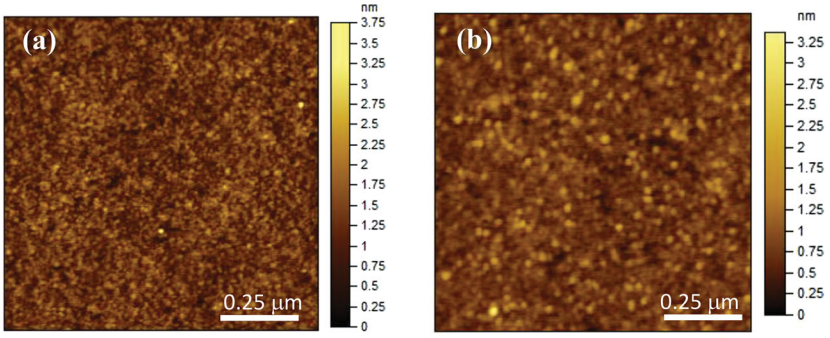

Figure 2. AFM topographic images of CFO thin films on a) STO (100) and b) STO (110).

beam epitaxy, and even atomic layer deposition after a post annealing treatment.[11,18,40,41] In our case, the stabilization of the Co-rich phase is promoted by the crystalline substrate that can induce epitaxial growth, as previously shown in other complex phases.[16,17,42] Uniquely, the atomic-scale degree of homogeneity along with the low kinetics achieved when using ALD may ensure the epitaxial growth at temperatures much lower (250 °C) than those obtained when using other thin-film deposition techniques (600–900 °C).[34,41,43,44]

The surface morphology of the CFO films was evaluated from atomic force microscopy (AFM). Topographic images of 10 nm CFO thin films on STO (100) and STO (110) are shown in **Figure 2**a,b, respectively. An ultra smooth surface roughness, rms ≈0.3 nm, is obtained for the two systems with no variation for different film thicknesses, as expected from a self-limited surface reaction. High resolution TEM images of the 10 nm thin films grown on STO (100) and on STO (110), **Figure 3**a,b, respectively, show that the CFO films are continuous over long lateral length and highly epitaxial. From the corresponding selected-area electron diffraction (SAED) patterns a cube on cube epitaxial relationship between the CFO film and the STO substrate is observed. The splitting of the film and the substrate diffraction spots are consistent with a fully relaxed film, in good agreement with our XRD data. The most common defects in cobalt ferrite spinel thin films are the antiphase boundaries (APBs),[18,45] which are understood as stacking defects of the atomic planes in the spinel lattice corresponding to a half lattice translation of the cationic sublattice.[18,45] It is worth noting that in our spinel films APBs are present in relatively high concentrations, see Figure 3c, which is expected to have a strong influence on the magnetic properties, specially in ultrathin films, as it will be discussed below. The high-resolution image of a 10 nm CFO film on STO (110) shows in detail the interface between an APB and the spinel structure. APBs show a different contrast because they comprise a half lattice shift of the cationic sublattice. The same defect is observed in all CFO/STO thin films, although the 5 nm CFO films contain higher concentrations of APB.

The chemical composition of CFO films with 5 nm and 15 nm thicknesses on both substrates STO (100) and STO (110) has been investigated by ex-situ X-ray photoelectron spectroscopy. From the survey spectra the presence of Co, Fe, O, Sr, and Ti is identified, consistent with the species pulsed onto the STO substrate (Supporting Information, Figure S3). High resolution XPS spectra of Co(2p) and Fe(2p) areas have been acquired for these set of samples, see **Figure 4**. Quantitative analysis of the cation ratio lead to 2Co:1Fe, in well agreement with the expected stoichiometry in Co_2FeO_4, see Supporting Information, Figure S4 and Table S1. All the films, regardless of thickness and orientation, show a similar chemical composition. High resolution Fe(2p) spectra, Figure 4a, show two main peaks attributed to the spin-orbit doublets $2p_{3/2}$ and $2p_{1/2}$. Fe $2p_{3/2}$ has a binding energy of 710.8 eV, very close to what has been previously reported for Co-Fe spinels and Fe_2O_3 phases.[46,47] Despite the weakness of the satellite peak at 718.8 eV characteristic of Fe^{3+}, the absence of Fe $2p_{3/2}$ peak asymmetries centered at 708 eV that could reveal the presence of Fe^{2+} ions suggests that the presence of Fe^{3+} species dominates. The Co(2p) line shapes are shown in Figure 4b. The $Co2p_{3/2}$ binding energy appears at 780.4 eV with satellite peaks situated 6 eV above the main peaks, in agreement with the structure reported for the spinel Co ferrites.[47–49] The presence of these satellite peaks is characteristic of Co^{2+} species, however, the satellite positions are not sufficiently chemically shifted and intense to allow ready

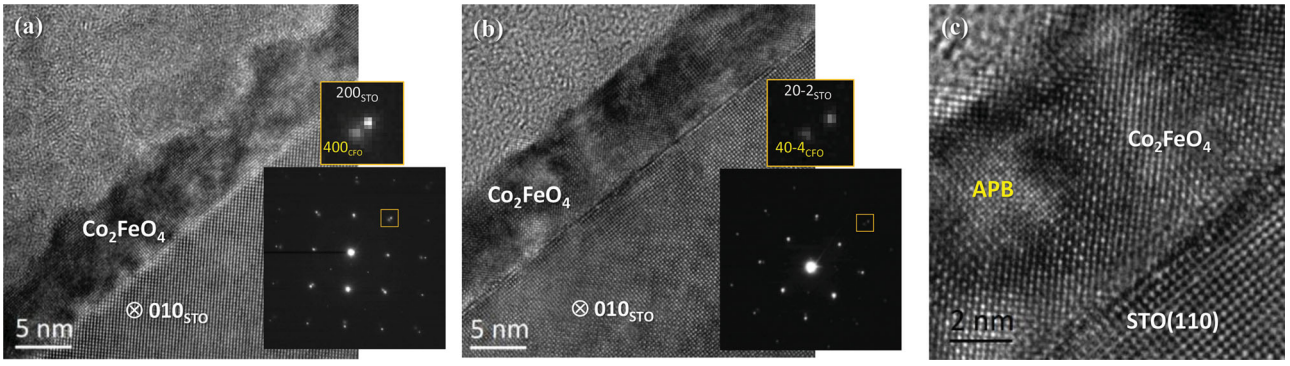

Figure 3. Cross-section bright-field high resolution TEM images of samples grown on a) STO (001) and b) STO (110), viewed along the zone axis [010] of STO. Insets show the corresponding SAED patterns. The indexed diffraction spots of the CFO layer and the substrate appear in yellow and white, respectively. c) Cross-section bright-field high-resolution TEM image of the 10 nm sample grown on STO (110) viewed along the zone axis [010] of STO identifying the presence of antiphase boundaries (APB).

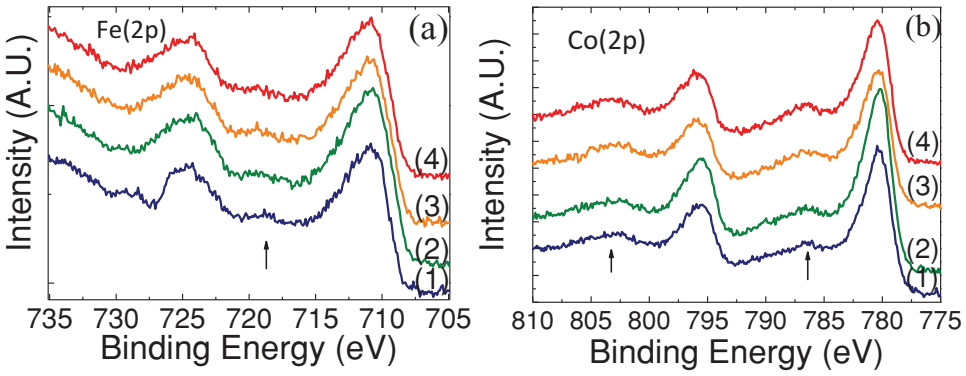

Figure 4. High resolutuion XPS spectra of a) Fe(2p) and b) Co(2p) regions for (1) 5 nm CFO on STO (110), (2) 5 nm CFO on STO (100), (3) 15 nm CFO on STO (110), and (4) 15 nm CFO on STO (100). Arrows indicate the position of the satellite peaks.

deconvolution of Co^{2+} and Co^{3+} species. Thus, XPS analysis confirms the cation ratio 2Co:1Fe and the presence of Fe^{3+} in our ALD films. Advanced characterization using a synchrotron light source would be required to understand the cation distribution in more detail.[18]

The magnetic behavior of as-deposited CFO thin films with various thicknesses has been evaluated. **Figure 5** shows the hysteresis loops at 10 K of 25, 10, and 5 nm CFO thin films on STO (100) with the field applied along the [100] direction, in-plane, and along the [001] direction, out-of-plane. It is observed that in-plane and out-of-plane hysteresis loops of 25 nm and 10 nm CFO thin films show almost no difference in remanence (M_r) and coercive field (H_c), Figure 5a,b, respectively. This behavior is in contrast to the easy magnetization axis typically reported for $CoFe_2O_4$ thin films,[28,29] which has been mainly attributed to the strain originating from the lattice mismatch with the substrate and could be accentuated by the film thickness and the processing temperature.[40,41,44,47,50] The contribution of the stress anisotropy to the magneto-crystalline anisotropy is given by $3\lambda_{100}\sigma/M_s$, where λ_{100} is the magnetostriction coefficient, σ is the uniaxial stress, and M_s is the saturation magnetization.[51] Based on our XRD and TEM data that showed the formation of fully relaxed films, the nearly equal in-plane and out-of-plane magnetization curves indicate that there is no modification of the magneto-crystalline anisotropy from the stress anisotropy. However, only for the 5 nm CFO films (Figure 5c), the shape of the hysteresis loop is significantly different. The in-plane H_c value is much higher than the out-of-plane, yet M_r is maintained. Note that these films are also fully relaxed (Figure 3a,b), which rules out a stress-induced magnetic anisotropy effect. Interestingly, as the CFO thickness decreases, a shrinking at low fields is more evident. This shrinkage observed at low fields, being particularly dramatic for the 5 nm films, has been observed in $CoFe_2O_4$ films on STO and MgO substrates. Some authors have assigned this behavior to the presence of two different magnetic phases.[44,52] Others have attributed this to the presence of APB that could weaken the magnetic interaction. They observed that the effect is stronger for thinner films because the concentration of APB is higher.[18] Therefore, according to our TEM observations it is likely that the shrinkage observed in the ALD stabilized Co_2FeO_4 thin films can be attributed to the high density of APB.

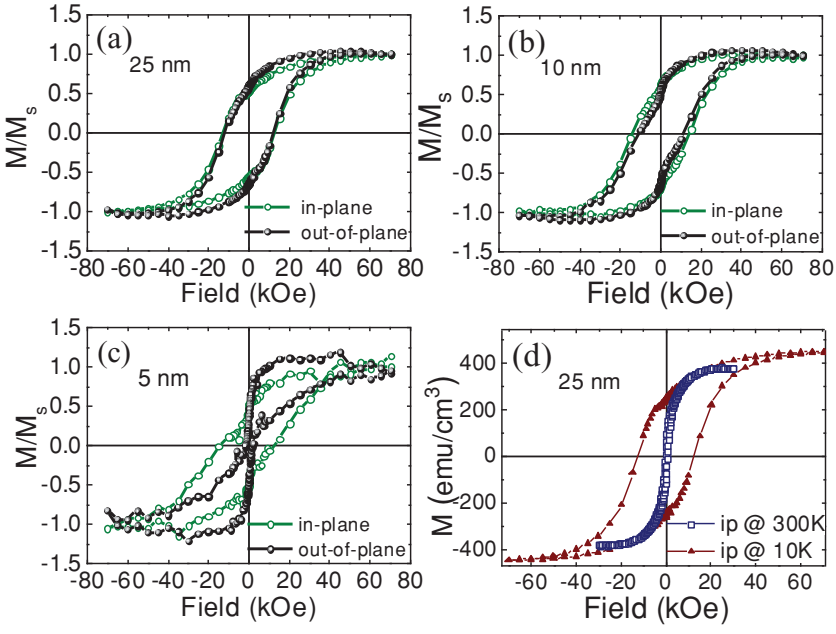

Figure 5. Magnetic hysteresis of as-deposited CFO thin films on STO (100) deposited at 250 °C: a) 25 nm, b) 10 nm, and c) 5 nm, measured at 10 K with the magnetic field applied along the in-plane (green open symbols) and out-of-plane (black solid symbols) direction. d) 25 nm CFO on STO(100) measured at 300 K (blue open symbols) and 10 K (red solid symbols) with the magnetic field applied along the in-plane direction.

The saturation magnetization (M_s) of CFO films with a thickness down to 10 nm is ≈450 emu cm^{-3} (≈3.3 μ_B per formula unit), slightly higher than the theoretical value expected for Co_2FeO_4.[8,10,12] Remanent magnetization of around 50% is observed for the whole range of film thicknesses. Based on these experimental values of M_s, the following cation distribution in the spinel structure $(Co^{2+}_{1-x}\ Fe^{3+}_{x})_A\ (Co^{2+}Fe^{3+}_{x}\ Co^{3+}_{1-x})_B\ O_4$ (with $0.16 < x < 0.4$) is proposed, where A and

B stand for the tetrahedral and octahedral cations sites in the cubic spinel structure, respectively. This distribution is in good agreement with the cation allocation previously reported based on diffraction, magnetic and spectroscopic experiments.[12,13,53] Also, H_c is close to 15 kOe, characteristic of a hard magnet when measuring along a hard axis direction.[31] For 5 nm films, M_s decreases to ≈230 emu cm^{-3} with coercive fields of 11 kOe and 2 kOe for parallel and perpendicular directions, respectively. Variations of the magnetic properties from the theoretical values are very common in spinel ferrite thin films.[8] For instance, a similar decrease of the magnetization and coercivity at low thicknesses has already been observed in Fe_3O_4 or $CoFe_2O_4$ on Mg(001) and has been attributed to the increased number of APBs,[45,54] consistent with the microstructural scenario found in our ALD films as anticipated above. Nonetheless, these ultrathin films offer many attractive applications in sensors, microelectronics, and spintronics. In Figure 5d, a comparison of 300 K and 10 K hysteresis loops of 25 nm CFO films on STO (100) is presented. Similar to the measurements performed at 10 K, the magneto-crystalline anisotropy of the Co_2FeO_4 phase at 300 K is not modified by the stress anisotropy although a smaller saturation magnetization (380 emu cm^{-3}) and a substantial coercive field decrease (0.5 kOe) is observed. The magnetic anisotropy constant (K_1) has been estimated at 300 and 10 K for the 25 and 15 nm thin films resulting in ≈4×10^6 erg cm^{-3} (300 K) and ≈10×10^6 erg cm^{-3} (10 K), on the same order of magnitude as the data obtained for bulk and thin film Co-ferrite samples.[41,55] Note that the decrease of H_c at 300 K is significantly higher than what would be expected based on K_1, which has already been observed in other cobalt-ferrite systems.[7,13,52] Finally, the 5 nm ALD-Co_2FeO_4 films also exhibit a smaller H_c at 300 K (0.2 kOe), following the same trend as observed at 10 K in Figure 5c, which is attributed to a higher density of APBs in ultrathin films.[18,45]

Analogously, the magnetic behavior of CFO films on STO (110) shows the same trend as CFO on STO (100) (Supporting Information, Figure S5). Note that in-plane measurements performed for the (0ll) oriented CFO films at 10 K at two different angles, 0° and 90°, show the same behavior indicating that the magneto-crystalline anisotropy along the hard axes <110> and <100> is the same.[55] The magnetism of Co_2FeO_4 layers could be further improved to be used as tunnel barriers when using substrates with better lattice matching (i.e., Pt (111), $MgAl_2O_4$ (001)). In these systems it is expected that, similar to what has been observed in $CoFe_2O_4$, the density of APBs will be lower.[18]

Thus, we have proven that highly epitaxial cobalt iron spinel oxide prepared by ALD at 250 °C with enhanced magnetic properties can be stabilized for thicknesses down to 10 nm. Thinner films, although highly crystalline, show slightly decreased magnetic properties. These variations cannot yet be clearly explained but it is likely that the presence of high density APB structural defects that break the crystalline order could be a key parameter.[6,45,47,56,57]

3. Conclusion

We have demonstrated the heteroepitaxial stabilization of the magnetic and metastable Co_2FeO_4 spinel phase at 250 °C using atomic layer deposition. Importantly, this low temperature process with atomic scale homogeneity has a direct impact on many critical film parameters including roughness, strain, crystallinity, and the magnetic properties. The ALD-Co_2FeO_4 films (5–25 nm) are highly epitaxial and fully relaxed with an ultrasmooth surface whereas traditional deposition techniques require high processing temperatures (600–900 °C) or post annealing treatments to achieve such characteristics. In addition, these ALD-Co_2FeO_4 films show enhanced magnetization and coercivity compared to the bulk values. Ultrathin films, similar to other ferrite layers, show a reduced magnetization and coercivity that might be attributed to a higher density of structural defects (APBs). Further improvement of the Co_2FeO_4 magnetic properties could be pursued by inducing the epitaxial stabilization with a substrate with smaller lattice mismatch. This low-cost and low-temperature process is a major step forward to prepare and stabilize epitaxial complex oxides with nanometric scale control, especially when the temperature is the main limitation. Furthermore, it holds promising implications for a large variety of materials, to integrate dissimilar layers and fabricate advanced devices even on 3D substrates, without compromising the system stability.

4. Experimental Section

ALD of Co_2FeO_4 Films: Co_2FeO_4 films were prepared in a Cambridge Nanotech Savannah flow-type reactor at 250 °C by alternate pulsing of cobaltocene ($Co(Cp)_2$) and ferrocene ($Fe(Cp)_2$) combined with ozone (O_3) to obtain the required film stoichiometry (2Co:1Fe). The number of supercycles was modified according to the desired film thickness (from 5 to 25 nm). The samples were prepared on 5 × 5 mm^2 (100) strontium titanate $SrTiO_3$ (STO) and (110) STO substrates previously cleaned by 5 min sonication in ethanol and dry N_2. Each run was performed simultaneously on STO(100), STO(110), and thermally grown SiO_2/Si (100) substrates. We have observed that for the three systems, the thickness of the CFO films depends linearly on the number of cycles, obtaining a constant growth rate of 0.5 Å/supercycle at 250 °C (Supporting Information, Figure S1). No subsequent heat treatment has been performed for the samples shown here.

Co_2FeO_4 Characterization: The film purity and crystallinity were studied using Rigaku Rotaflex RU-200BV X-ray diffractometer with Cu-K_α λ = 1.5418 Å. Texture analysis was perfomed using a XRD^2 GADDS D8 Advance system from Bruker. X-ray in-plane reciprocal space maps were obtained with a φ-$2\theta/\omega$ configuration using a Panalytical X´Pert PRO MRD instrument (CuK_α radiation and PIXel detector) at the Institut Català de Nanociència i Nanotecnologia (CIN2), Barcelona, Spain. The surface morphology was evaluated by scanning force microscopy with a microscope 5500 from Agilent Technologies. The surface chemical composition was studied by Kratos Axis Ultra X-ray Photoelectron Spectroscopy with a Mg K_α source (1253.6 eV), a pass energy of 160 eV for survey spectra and 20 eV for high resolution spectra, at the Instituto de Nanociencia de Aragon (INA), Zaragoza, Spain. To compensate charging effects, all spectra were calibrated respect to the C(1s) peak at 284.9 eV. Transmission electron microscopy (TEM) images and selected-area electron diffraction (SAED) patterns have been acquired using a FEI Tecnai G^2 F20 operated at 200 kV. TEM specimens were thinned by mechanical grinding, polishing, and dimpling, followed by Ar-ion milling. Macroscopic magnetic measurements were performed at 300 and 10 K using a Quantum Design superconducting quantum interference device SQUID. The magnetic field is applied along the [100] direction (in-plane) and [001] direction (out-of-plane) varying

from 0 to 7 T, M(H). The magnetization curves were corrected from the STO diamagnetic contribution.

Supporting Information

Supporting Information is available from the Wiley Online Library or from the author.

Acknowledgements

This research was supported by MAT2011–28874-C02–01 and Consolider. M.C. acknowledges the JdC Spanish MICINN grant and J.G. acknowledges the RyC-201211709 contract. The authors gratefully acknowledge financial support from the German Research Foundation (DFG) via SFB 986 "M^3", project C3. They acknowledge the use of the X-ray photoelectron spectroscopy infrastructure available in the Laboratorio de Microscopias Avanzadas (LMA) at the Instituto de Nanociencia de Aragon (University of Zaragoza, Spain) and the Scientific Services at ICMAB. The TEM microscopy work and high resolution XRD was conducted in the Catalan Institute of Nanoscience and Nanotechnology (ICN2). The authors acknowledge the ICN2 Electron Microscopy Division for offering access to their instruments and expertise.

Received: February 14, 2014
Revised: March 27, 2014
Published online: June 10, 2014

[1] *Advances in Ferrites*, (Ed: M. C. Srivastava, M. Patni), Trans Tech Publications, Aedermannsdorf, Switzerland **1990**.
[2] Y. Suzuki, *Annu. Rev. Mater. Res.* **2001**, *31*, 265.
[3] V. A. M. Brabers, *Handbook of Magnetic Materials*, North-Holland Publishing Company, Amsterdam, The Netherlands **1982**.
[4] J. W. Sun, Y. S. Fu, P. Xiong, X. Q. Sun, B. H. Xu, X. Wang, *RSC Adv.* **2013**, *3*, 22490.
[5] H. Zheng, J. Wang, S. E. Lofland, Z. Ma, L. Mohaddes-Ardabili, T. Zhao, L. Salamanca-Riba, S. R. Shinde, S. B. Ogale, F. Bai, D. Viehland, Y. Jia, D. G. Schlom, M. Wuttig, A. Roytburd, R. Ramesh, *Science* **2004**, *303*, 661.
[6] U. Luders, M. Bibes, J. F. Bobo, M. Cantoni, R. Bertacco, J. Fontcuberta, *Phys. Rev. B* **2005**, *71*, 134419.
[7] J. C. Slonczewski, *J. Phys. Chem. Solids* **1961**, *18*, 269.
[8] A. Walsh, S. H. Wei, Y. Yan, M. M. Al-Jassim, J. A. Turner, *Phys. Rev. B* **2007**, *76*, 165119.
[9] L. F. Liotta, G. Di Carlo, G. Pantaleo, G. Deganello, *Appl. Catal. B: Environ.* **2007**, *70*, 314.
[10] T. A. S. Ferreira, J. C. Waerenborgh, M. H. R. M. Mendonca, M. R. Nunes, F. M. Costa, *Solid. State Sci.* **2003**, *5*, 383.
[11] M. Lie, K. B. Klepper, O. Nilsen, H. Fjellvag, A. Kjekshus, *Dalton Trans.* **2008**, 253.
[12] I. P. Muthuselvam, R. N. Bhowmik, *Solid State Sci.* **2009**, *11*, 719.
[13] M. Takahash, M. E. Fine, *J. Appl. Phys.* **1972**, *43*, 4205.
[14] N. Tristan, V. Zestrea, G. Behr, R. Klingeler, B. Buchner, H. A. K. von Nidda, A. Loidl, V. Tsurkan, *Phys. Rev. B* **2008**, *77*, 094412.
[15] A. A. Bosak, A. A. Kamenev, I. E. Graboy, S. V. Antonov, O. Y. Gorbenko, A. R. Kaul, C. Dubourdieu, J. P. Senateur, V. L. Svechnikov, H. W. Zandbergen, B. Holländer, *Thin Solid Films* **2001**, *400*, 149.
[16] D. Meyers, E. J. Moon, M. Kareev, I. C. Tung, B. A. Gray, J. Liu, M. J. Bedzyk, J. W. Freeland, J. Chakhalian, *J. Phys. D: Appl. Phys.* **2013**, *46*, 385303.
[17] P. A. Salvador, T. D. Doan, B. Mercey, B. Raveau, *Chem. Mater.* **1998**, *10*, 2592.
[18] J. B. Moussy, *J. Phys. D: Appl. Phys.* **2013**, *46*, 143001.
[19] G. N. Parsons, S. M. George, M. Knez, *MRS Bull.* **2011**, *36*, 865.
[20] *Atomic Layer Deposition of Nanostructured Materials*, (Ed: N. Pinna, M. Knez), Wiley-VCH, Weinheim, Germany **2012**.
[21] X. Wang, L. Dong, J. Zhang, Y. Liu, P. Ye, R. Gordon, *Nano Lett.* **2013**, *13*, 594.
[22] V. Miikkulainen, M. Leskela, M. Ritala, R. L. Puurunen, *J. Appl. Phys.* **2013**, *113*, 021301.
[23] P. A. Hansen, H. Fjellvag, T. Finstad, O. Nilsen, *Dalton Trans.* **2013**, *42*, 10778.
[24] V. Miikkulainen, O. Nilsen, M. Laitinen, T. Sajavaara, H. Fjellvag, *RSC Adv.* **2013**, *3*, 7537.
[25] E. Ostreng, H. H. Sonsteby, T. Sajavaara, O. Nilsen, H. Fjellvag, *J. Mater. Chem. C* **2013**, *1*, 4283.
[26] A. R. Akbashev, G. Chen, J. E. Spanier, *Nano Lett.* **2014**, *14*, 44.
[27] W. M. Li, *Chem. Vap. Deposition* **2013**, *19*, 82.
[28] H. J. Fan, M. Knez, R. Scholz, K. Nielsch, E. Pippel, D. Hesse, M. Zacharias, U. Gosele, *Nat. Mater.* **2006**, *5*, 627.
[29] H. J. Fan, M. Knez, R. Scholz, D. Hesse, K. Nielsch, M. Zacharias, U. Gosele, *Nano Lett.* **2007**, *7*, 993.
[30] G. Armelles, A. Cebollada, A. García-Martín, J. M. Montero-Moreno, M. Waleczek, K. Nielsch, *Langmuir* **2012**, *28*, 9127.
[31] Y. T. Chong, E. M. Y. Yau, K. Nielsch, J. Bachmann, *Chem. Mater.* **2010**, *22*, 6506.
[32] Y. T. Chong, M. Y. E. Yau, Y. Yang, M. Zacharias, D. Gorlitz, K. Nielsch, J. Bachmann, *J. Appl. Phys.* **2011**, *110*, 043930.
[33] C. Wiemer, L. Lamagna, M. Fanciulli, *Semicond. Sci. Technol.* **2012**, *27*, 074013.
[34] M. Coll, J. Gazquez, A. Palau, M. Varela, X. Obradors, T. Puig, *Chem. Mater.* **2012**, *24*, 3732.
[35] M. Coll, A. Palau, J. Gonzalez-Rosillo, J. Gazquez, M. Varela, X. Obradors, T. Puig, *Thin Solid Films* **2014**, *553*, 7.
[36] K. B. Klepper, O. Nilsen, H. Fjellvag, *J. Crystal Growth* **2007**, *307*, 457.
[37] Y. D. Shen, Y. W. Li, W. M. Li, J. Z. Zhang, Z. G. Hu, J. H. Chu, *J. Phys. Chem. C* **2012**, *116*, 3449.
[38] T. Ngo, A. Posadas, M. McDaniel, D. Ferrer, J. Bruley, C. Breslin, A. Demkov, J. Ekerdt, *J. Crystal Growth* **2013**, *363*, 150.
[39] K. Uusi-Esko, M. Karppinen, *Chem. Mater.* **2011**, *23*, 1835.
[40] X. S. Gao, D. H. Bao, B. Birajdar, T. Habisreuther, R. Mattheis, M. A. Schubert, M. Alexe, D. Hesse, *J. Phys. D: Appl. Phys.* **2009**, *42*, 175006.
[41] P. D. Thang, G. Rijnders, D. H. A. Blank, *J. Magn. Magn. Mater.* **2007**, *310*, 2621.
[42] K. Uusi Esko, J. Malm, M. Karppinen, *Chem. Mater.* **2009**, *21*, 5691.
[43] A. V. Ramos, *PhD thesis*, Université Pierre et Marie Curie, **2008**.
[44] F. Rigato, J. Geshev, V. Skumryev, J. Fontcuberta, *J. Appl. Phys.* **2009**, *106*, 113924.
[45] D. T. Margulies, F. T. Parker, M. L. Rudee, F. E. Spada, J. N. Chapman, P. R. Aitchison, A. E. Berkowitz, *Phys. Rev. Lett.* **1997**, *79*, 5162.
[46] N. S. McIntyre, D. G. Zetaruk, *Anal. Chem.* **1977**, *49*, 1521.
[47] A. V. Ramos, T. S. Santos, G. X. Miao, M. J. Guittet, J. B. Moussy, J. S. Moodera, *Phys. Rev. B* **2008**, *78*, 180402.
[48] N. S. Mcintyre, M. G. Cook, *Anal. Chem.* **1975**, *47*, 2208.
[49] Y. Q. Chu, Z. W. Fu, Q. Z. Qin, *Electrochim. Acta* **2004**, *49*, 4915.
[50] A. Lisfi, C. M. Williams, *J. Appl. Phys.* **2003**, *93*, 8143.
[51] P. C. Dorsey, B. J. Rappoli, K. S. Grabowski, P. Lubitz, D. B. Chrisey, J. S. Horwitz, *J. Appl. Phys.* **1997**, *81*, 6884.
[52] L. Horng, G. Chern, M. C. Chen, P. C. Kang, D. S. Lee, *J. Magn. Magn. Mater.* **2004**, *270*, 389.

[53] X. Batlle, X. Obradors, J. Rodriguezcarvajal, M. Pernet, M. V. Cabanas, M. Vallet, *J. Appl. Phys.* **1991**, *70*, 1614.
[54] S. Matzen, J. B. Moussy, R. Mattana, F. Petroff, C. Gatel, B. Warot-Fonrose, J. C. Cezar, A. Barbier, M. A. Arrio, P. Sainctavit, *Appl. Phys. Lett.* **2011**, *99*, 052514.
[55] R. M. Bozorth, E. F. Tilden, A. J. Williams, *Phys. Rev.* **1955**, *99*, 1788.
[56] S. Xie, J. Cheng, B. W. Wessels, V. P. Dravid, *Appl. Phys. Lett.* **2008**, *93*, 181901.
[57] J. X. Ma, D. Mazumdar, G. Kim, H. Sato, N. Z. Bao, A. Gupta, *J. Appl. Phys.* **2010**, *108*, 063917.